Carbon fibre fluorination: Surface and structural properties

Jean-Charles Agopian, Olivier Téraube, Karine Charlet, Samar Hajjar-Garreau, Elodie Petit, Nicolas Batisse, Marc Dubois

Version of Record: https://www.sciencedirect.com/science/article/pii/S0169433222011138
Manuscript_a055680390dee5e8f74c9443dd37bb0b

Carbon fibre fluorination: surface and structural properties

Jean-Charles Agopian*[a], Olivier Téraube[b], Karine Charlet[a], Samar Hajjar-Garreau[c], Elodie Petit[b], Nicolas Batisse[b], Marc Dubois[b]

*: corresponding author. Tel: +33675182245. E-mail: jean-charles.agopian@sigma-clermont.fr.

[a] Université Clermont Auvergne, Clermont Auvergne INP, CNRS, Institut Pascal, F-63000 Clermont–Ferrand, France.

[b] Université Clermont Auvergne, Clermont Auvergne INP, CNRS, ICCF, F-63000 Clermont–Ferrand, France.

[c] Institut de Sciences des Matériaux de Mulhouse, CNRS-UMR 7361, Université de Haute Alsace, 68100 Mulhouse, France.

Abstract: Knowing that carbon fibre reinforced polymers are sensitive to moisture through their interphases, carbon fibres sized with Bisphenol A diglycidyl ether were fluorinated under a N_2/F_2 atmosphere, which confers them a hydrophobic behaviour, as highlighted by wettability measurements. Low fluorination temperatures (< 230°C) lead to a sizing perfluorination and even overfluorination without carbon fibre fluorination, while higher temperatures (> 250°C) result in a carbon lattice fluorination with a complete desizing of the fibre through decomposition, that has been evidenced through X-Ray Diffraction and Raman spectroscopy studies. For both fluorination mechanisms, ^{19}F Nuclear Magnetic Resonance, X-Ray Photoelectron and infrared spectroscopy have been used to study the nature of fluorine bonds. Scanning Electron Microscope and Energy-Dispersive X-Ray Spectroscopy have evidenced a core-shell structure for the fluorinated fibres with a fibre degradation at the highest temperatures, also highlighted by tensile tests, Atomic Force Microscopy and Electron Paramagnetic Resonance.

Keywords: Fluorination; Carbon fibers; Surface and Bulk Properties; XPS; Wettability.

1 Introduction

Carbon fibres own outstanding mechanical properties, as they have the highest strength and specific modulus amongst fibres [1]. They are extensively used to reinforce epoxy-based composite materials [2], in various industries, *e.g.* aerospace or nuclear [3]. Due to their chemical inertness, carbon fibres are coated with sizing, a thin polymer layer, for further use with epoxy matrix [4,5]. This treatment has an influence on the composite mechanical properties and allows to reach an optimal fibre/matrix adhesion [6,7]. During the composite lifetime, moisture absorption at the fibre/matrix interphase can nevertheless lower this adhesion and decrease the interfacial shear strength [8], which can lead to fibre debonding and composite mechanical weakening.

Reduction of moisture absorption can be achieved by giving a hydrophobic behaviour to carbon fibres. Several techniques have already been performed leading to hydrophobicity enhancement for carbonaceous materials. Some of them are based on intermolecular interactions through the grafting of non-polar alkyl groups onto the fibre surface, *e.g.* electrochemical reduction [9], soaking and spraying of fluoroplastics [10], or polytetrafluoroethylene (PTFE) suspension deposition [11]. It is also possible to modify the fibre morphology and roughness, by exploiting lotus-leaf effect through deposition of carbonaceous materials on other carbon lattice [9,12].

Fluorination is also a well-known approach to confer hydrophobic and barrier properties to a wide range of materials, such as polymers [13–15], carbons [16–19] or wood-based materials [20–22]. Fluorination thus appears as a promising solution to protect fibre/matrix interface from moisture absorption and to maintain interesting interfacial properties. In this study, sized fibres were fluorinated. As the objective was to graft fluorine atoms not only on the sizing, but also on the carbon lattice, a wide reaction temperature range in between 20 and 450°C was considered, meaning that a sizing burn is expected [23], which could lead to a fibre-matrix adhesion decrease, because of the presence of a not-adherent residual perfluorinated sizing [24]. It implies that temperatures sufficiently high are sought to completely remove the sizing in order to avoid such an adhesion loss. Sizing fluorination is however possible, and has already been studied [25].

Concerning the fluorination reaction mechanism, as the temperatures at stake are high, up to 450°C, fluorine atoms are expected to covalently bond to carbon, by breaking the double bonds of graphitic carbons and by the conversion of carbon hybridization from sp^2 to sp^3. This

evolution from graphitic to tetravalent carbons with the fluorination treatment has already been reported many times in various studies on fluorinated carbon fibres [16,17,26–28], or more widely on fluorinated carbonaceous (nano)materials [29–33]. For ordered carbons, this sp^2 to sp^3 conversion occurs under pure fluorine at high temperatures, at least 300°C [26], or more generally under strong fluorination conditions [17,34]. $(CF)_n$ and $(C_2F)_n$ structural types may be formed according to the temperature and duration. $(C_2F)_n$ with FCCF/FCCF stacking sequence is an intermediate phase in the 350-500°C range whereas $(CF)_n$ (FCF/FCF stacking) is formed at the highest temperatures up to 650°C [35]: the higher the temperature, the higher the fluorination level x (x = F:C, $0.5 < x < 1$) [36].

Fluorination exhibits several advantages over other surface functionalisation methods [37]:

- Direct fluorination (fluorination under molecular fluorine F_2) is a dry process, meaning that it does not require use and storage of often toxic solvents, while sizing treatments are wet processes. Moreover, optimised fluorination conditions lead to a low ecological footprint treatment, without human contact with the reactant [38].
- Safe methods exist to neutralise residual F_2 and fluorinated end-products in the fluorination reactor [15].
- Fluorination requires a strict control of the experimental conditions, allowing to reach controllable and repeatable properties on fluorinated materials.
- The versatility of the C-F bond nature allows to reach an extraordinary diversity of properties for fluorinated materials, but requires a good understanding and control of both the experimental conditions and the starting material.
- Most fluorination processes, especially direct fluorination, may be performed at the industrial scale, as proved by the fluorination of car tanks [39].
- If fluorination occurs at room temperature (RT), it is a low energy consuming reaction. Independently of the reaction temperature, as fluorine is highly reactive, it is a quick and spontaneous surface modification method with a high reaction yield.

Moreover, as it will be shown in this article, another benefit of this fluorination route is the possible tailoring of the fibre surface energy through a precise control of the reaction temperature. This could be a promising way to optimise the interaction between fluorinated fibres and various polymers, as the interfacial shear strength of a carbon fibres/hydrophobic polymer system has been found to evolve the same way than the γ_s^d/γ_s ratio, where γ_s^d is the dispersive component of the fibre surface energy and γ_s the fibre total surface energy [40].

Fluorination could thus be a functionalising method competing with sizing, allowing more versatility than sizing treatment, which depends of the chosen coupling agent.

Fluorination of the carbon lattice can also avoid moisture absorption at the fibre/matrix interface, while still ensuring a good adhesion between the reinforcement and the matrix. In this study, the effects of fluorination on the carbon fibres will be investigated in order to define the treatment conditions to reach a slight fluorination of the carbon lattice, without huge over-fluorination and losses of mechanical performances.

2 Materials and methods

2.1 Materials

Carbon fibre fabric is a HiMax^{TM} FCIM 313 from Hexcel. With ^{1}H Nuclear Magnetic Resonance (NMR), Attenuated Total Reflectance - Infrared Spectroscopy (ATR-IR) and Mass Spectrometry analyses, the sizing main pre-polymer has been identified as Bisphenol A diglycidyl ether (DGEBA). DGEBA belongs to the most widely used epoxy-resin family, the diglycidyl ethers [41].

For comparison, fibres were desized by a Soxhlet extraction in acetone for 48h and dried for 24h at 60°C in a Buchi vacuum drier (10^{-3} mbar) [16,18,23]. The objective was not to fluorinate these fibres, but rather to have a comparison between desized non-fluorinated and sized fluorinated fibres, the latter ones being possibly desized by the fluorination treatment.

The resin used for tensiometric measures was the 1050 epoxy resin from Resoltech, combined with their 1056S hardener in 100:35 proportions

2.2 Fluorination

Samples for fluorination consisted of 8 carbon fibre bundles which were 10 cm long, each bundle containing 12 000 fibres. The glass weft yarns, which ensured the maintaining of the carbon bundles together, were not removed before the fluorination process.

Samples were treated with static fluorination. Fluorination apparatus, described in Figure SI 1, given in Supporting Information, consists of a reactor linked to a pure fluorine gas (F_2, 99.9% purity provided by Solvay) and a nitrogen gas (N_2, 99.999% purity) bottles. A trap containing soda lime (10% NaOH + 80% $Ca(OH)_2$ + 10% KOH) is set up at the reactor output, in order to trap residual F_2 molecules.

Carbon bundles were put in a passivated-nickel basket (covered with NiF_2 layer), which was placed at a specific position in the reactor to ensure the fluorination reproducibility. The reactor was then closed, and vacuum (10^{-3} bar) was applied in it. The pump valve was then switched off, meaning the reactor was a closed system, and different fluorination temperatures were applied: 20°C, 140°C, 230°C, 250°C, 280°C, 310°C, 330°C, 380°C, and 450°C.

Throughout this article, samples will be designated as follows: FCF-T, FCF meaning Fluorinated Carbon Fibre, and T being the fluorination temperature (*e.g.* FCF-250). For non-fluorinated fibres, the sized ones will be designed as Sized Non-F and the desized ones as Desized Non-F.

N_2 was first introduced up to a pressure of 0.03 MPa and then molecular fluorine up to 0.06 MPa. Atmospheric pressure (0.1 MPa) was reached with N_2. Once this pressure was reached, N_2 valve was switched off, and 20 minutes were timed. The valve between the reactor and the soda lime trap was then opened, the temperature regulation was switched off, and the reactor was flushed for at least 2 hours with N_2 (flux of 600 mL/min) in order to eliminate both the remaining fluorine and side products (*e.g.* HF, CF_4). The carbon fibre bundles were then removed from the reactor, while avoiding any HF release, for further characterisation.

Concerning the treatment homogeneity, as the fluorination process is a gas/solid reaction starting from vacuum, all surfaces reachable by fluorine are reacting. This assumption can notably be checked through the homogeneity of volume analyses, such as ^{19}F solid state Nuclear Magnetic Resonance (^{19}F NMR).

2.3 Characterisation

Fibres were extensively studied through surface and bulk characterisations. Surface ones include Energy-dispersive X-ray spectroscopy (EDX), Scanning Electron Microscopy (SEM), Attenuated Total Reflectance Infrared (ATR-IR), X-Ray Photoelectron Spectroscopy (XPS), Atomic Force Microscopy (AFM), and wettability, Specific Surface Area (SSA) and tribology measurements. Bulk ones include X-Ray Diffraction (XRD), Raman spectroscopy, ^{19}F NMR, Electron Paramagnetic Resonance (EPR), Thermo-Gravimetric Analyses (TGA), Mass Spectroscopy (MS), and tensile tests, the latter apparatus being illustrated in Figure SI 2. Details on each analysis are also given in Supporting Information.

3 Results and discussion

3.1 Fluorinated fibre aspect

For fluorination temperatures up to 250°C, fluorinated fibres keep the same shiny black colour as the Non-F ones. Above 250°C, interference phenomena appear and fluorinated fibres exhibit green and purple reflects as a function of the vision angle (Figure SI 3a), evidencing advanced fluorination and the variety of formed compounds [16]. FCF-450 sample turns black again while its edges become white, showing intense fluorination conditions [42,43]. UV-visible spectrometry measurements were carried out on Non-F sized fibres and FCF-310 sample and are given in Figure SI 3b. The similarity between both spectra ensures that fluorinated fibres do not absorb more than the Non-F sized ones, and that interferences are coming from a wavelength-related reflection difference, which is due to the fluorinated fibre microtexture.

3.2 Structural evolutions induced by fluorination

In order to characterise the structural evolutions induced by fluorination, ATR-FTIR analyses have first been carried out in Figure 1a. Non-F sized fibres exhibit several bands which have been attributed to the DGEBA sizing [25], whose vibration band assignment is proposed in Table SI 1. The reference bands are the ones commonly used to follow the evolution of DGEBA chemical change during a treatment, such as curing [44].

For low fluorination temperatures (20-140°C), it highlights a fluorination of the sizing, with the increase of the superimposed bands of vibration in C-Fx groups (C-F, CF_2 and CF_3) in the 900-1300 cm^{-1} range. FCF-230 sample then shows a complete desizing by the fluorine through degradative reactions between fluorine and sizing, but without any carbon fluorination. Fluorinations above 250°C lead to the emergence of a dissymmetric band at 1200 cm^{-1}, of mostly covalent C-F, and of a small band at 1320 cm^{-1}, this peak being attributed to CF_2 groups [45,46]. It should be also noted that FCF-140 sample exhibits a strong band at 1750 cm^{-1}, which can be attributed to -COOH groups, which could come either from the reaction of dangling bonds with oxygen and H_2O from air followed by hydrolysis, or from DGEBA degradation to esters, even though this mechanism has not been reported under fluorination conditions yet.

Spectra without subtraction of the background, given in Figure SI 4, show the evolution of the band intensity assigned to fluorinated species with the fluorination temperature. FCF-330 sample has the most intense contribution, while fibres fluorinated at higher temperatures

exhibit less intense bands. This could be due to the elimination of fluorine through exfoliation and formation of gaseous carbon fluorides, which indicates overfluorination and strongly degrades the fibres.

The dissymmetric band emerging for high-temperature fluorinated fibres of Figure 1a has been deconvoluted in two different components, one located at 1220 cm^{-1} being assigned to purely covalent C-F, while the one at 1180 cm^{-1} is due to semi-covalent C-F [30,47,48]. Their relative areas are indicated in Figure 1b, highlighting the increase of the covalent contribution with increasing temperature.

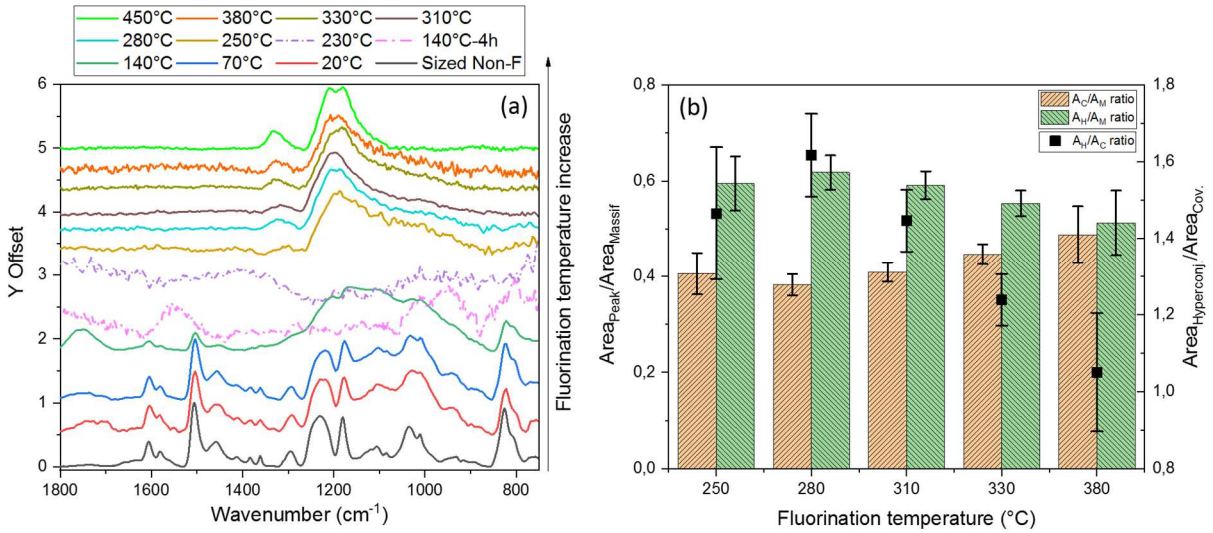

Figure 1: (a) Normalised infrared spectra of carbon fibres depending on fluorination temperature, (b) evolution of the ATR-FTIR peak relative areas depending on fluorination temperature *[print with colour]*

The analysis of infrared spectra evidences several fluorination mechanisms depending on the temperature; 230°C appears as the transition temperature between sizing and carbon fibre fluorination. ATR-FTIR analyses also highlight the increase of C-F covalence with the temperature increase in accordance with broadening of the fluorinated zones. In other words, C-F with weakened covalence because of their dilution in sp^2 lattice tend to disappear. A fluorine departure from the fibre, through the emission of gaseous fluorides and exfoliation phenomenon, is also underlined for high-temperature treatments by the intensity decrease of the band. The kinetic aspect of fluorination has also been investigated by fluorinating fibres at 140°C for 4h. The related ATR-FTIR spectrum highlights further polymer degradation than for the FCF-140 sample fluorinated for 20 minutes, but without complete desizing of the fibre (*e.g.* FCF-230 sample), as diffuse peaks are still observable. The transition between sizing and carbon fibre fluorination thus appears to be governed rather by temperature than by duration.

XRD analyses have then been realised and are given in Figure 2. The peak at 26° is assigned to the *002* reflection of the graphitic phase [49]. The peak at 10-15° that appears for treatment at 280°C is related to carbon fluorides, *001* reflection [16]. Its intensity decreases for fluorination temperatures above 330°C, strengthening the hypothesis of a departure of fluorinated species through the emission of gaseous fluorinated species and/or partial exfoliation, i.e. delamination of fluorocarbon phases from the carbon lattice.

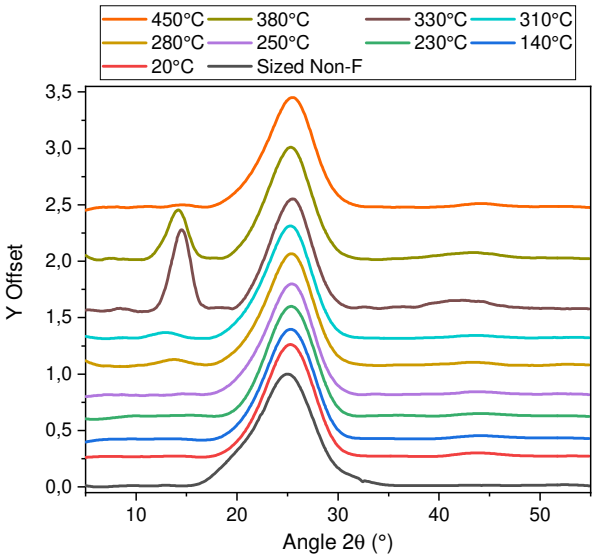

Figure 2: Normalised diffractograms of carbon fibres depending on fluorination temperature *[print with colour]*

By using the diffractograms and the Scherrer formula [50] for both phases, the interlayer distances *d* and coherence lengths L_C where extracted and are gathered in Table 1. Fluorination until 330°C remarkably increases the coherence length of the graphitic phase, which can be explained by the removal of amorphous carbon by fluorine, i.e. decomposition in volatile fluorinated species. Above this temperature, the coherence length decreases, which could be explained by a lattice reorganisation caused by a fluorine accommodation starting from the surface and progressing towards the core. Fluorination thus appears to focus preferentially on the less graphitised areas of the carbon fibre, as stated in [31].

Concerning the fluorocarbon layer stacking, its interlayer distance slightly above 6 Å underlines that the fluorinated phase is $(CF)_n$ rather than $(C_2F)_n$ (d_{001} = 8 Å) [47,51]. The coherence length along the c axis of fluorocarbon lattice increases with the temperature in accordance with a progression of the fluorination from the surface to the core and the removal of fluorinated amorphous carbons.

Table 1: Interlayer spaces and coherence lengths of fluorinated carbon fibres

Fluorination temperature (°C)	Sized Non-F	20	140	230	250	280	310	330	380	450
d_{002} (ang)	3.56	3.51	3.51	3.50	3.50	3.50	3.51	3.48	3.51	3.50
$L_{C\,002}$ (nm)	1.27	1.43	1.45	1.48	1.49	1.51	1.51	1.68	1.59	1.47
L_C evolution (%)	0	13	15	17	18	19	19	33	26	16
d_{001} (ang)	-	-	-	-	-	6.4	6.8	6.1	6.2	6.1
$L_{C\,001}$ (nm)	-	-	-	-	-	2.8	3.0	3.7	3.4	3.7

Structural evolutions have also been studied through Raman spectroscopy. The spectra, where fluorescence component is removed, are relatively similar and presented in Figure SI 5a. A two-band model has been used to deconvolute the Raman spectra, with a Breit-Wigner-Fano shape for the G band due to its asymmetry, and a Lorentzian shape for the D band [52]. A fitting example is given in Figure SI 5b. The G peak positions of the fluorinated carbon fibres are between 1580 cm^{-1} and 1600 cm^{-1}, highlighting that they belong to stage 1 or early-stage 2 according to the tree-stage model proposed by Ferrari and Robertson [53]. The Tuinstra and Koenig's relation [54,55] has thus been used to determine the coherence lengths La_T gathered in Table 2, where the I_D/I_G ratios are also reported, with the intensities referring to the peak heights [53].

Fluorination temperatures up to 230°C lead to a slight increase of the coherence length and a small decrease of the I_D/I_G ratio. These evolutions can be explained by a removal of the sizing and of the less organised carbons, which exhibit a high reactivity towards fluorine gas and are thus easy to eliminate, even at low temperatures. FCF-250 sample has the lowest I_D/I_G ratio (0.77 ± 0.01) and the highest coherence length (5.7 ± 0.1 nm): at this temperature, fluorine gas reacts mostly with the less organised areas of the fibres, contrary to the graphitic regions. When the fluorination goes further at higher temperatures, the organised carbon lattice is affected too, as evidenced by the changes of I_D/I_G ratio (increase) and coherence length (decrease).

Table 2: I_D/I_G ratio and coherence length of carbon fibres depending on fluorination temperature

Fluorination temperature (°C)	Sized Non-F	20	70	140	230	250	280	310	330	380
I_D/I_G	1.08 ± 0.01	1.05 ± 0.01	0.90 ± 0.01	1.04 ± 0.01	1.16 ± 0.01	0.77 ± 0.01	0.95 ± 0.01	1.02 ± 0.01	1.28 ± 0.1	0.97 ± 0.1
La_T (nm)	4.0 ± 0.1	4.2 ± 0.1	4.9 ± 0.1	4.2 ± 0.1	3.8 ± 0.1	5.7 ± 0.1	4.6 ± 0.1	4.3 ± 0.1	3.4 ± 0.1	4.5 ± 0.1

Raman spectra confirm that fluorination may act as a purification step by the removal of sizing and amorphous carbons. When the treatment is performed in mild conditions as for FCF-250 sample, the fibres are the most organised, as highlighted by both I_D/I_G ratio and coherence length.

The ^{19}F NMR spectra of fluorinated carbon fibres and sizing are given in Figure 3. Figure 3a evidences two distinct shapes according to the reaction temperatures, similarly to the ATR-FTIR spectra. Fibres fluorinated at the lowest temperatures (FCF-20 and FCF-70 samples) exhibit a high band at -190 ppm and a tiny one at -128 ppm, which can be assigned to C-F bonds and CF_2 groups [38]. These bands could be attributed to the fluorinated sizing. As a matter of fact, it can be seen that the intensity of the C-F peak decreases from 20°C to 70°C, while the one of the CF_2 one increases, showing a progression in the fluorine grafting. The spectrum of FCF-70 sample exhibits similarities with the one of fluorinated sizing; a similar fluorination could be obtained for these two samples. The sudden disappearance of those peaks for FCF-140 sample suggests that most of the sizing has been already perfluorinated and eliminated (overfluorinated) at this temperature, in accordance with the absence of band for FCF-230 sample (except the talc one). As ^{19}F NMR is a volume analysis, this absence of band for FCF-230 sample outlines the fluorination homogeneity assumed in section 2.2.

Fluorinations above 250°C lead to the emergence of various peaks, whose post-deconvolution attribution has been made in Table SI 2. Spinning sidebands are spaced of 30 000 Hz / 282 MHz i.e. 106 ppm. High amounts of CF_2 and CF_3 groups are characteristic of a fluorinated amorphous phase where the carbon sheets are of low lateral size. CF_2 and CF_3 groups can be formed only at the edges of graphene layer [56,57]. The high intensity of the CF_3 band for FCF-450 sample must be noted. Because CF_3 is the last fluorinated group formed before the emission of gaseous fluorides (CF_4 and C_2F_6) by addition of an additional fluorine atom, the content of CF_3 groups appears a valuable parameter to estimate the structural disorder and the decomposition rate. The higher their content, the more advanced the decomposition. Such a phenomenon is observed for porous carbons with high SSA and then high reactivity towards F_2 gas [58].

The deconvolution of the dissymmetric CF massif (-150 to -200 ppm) has been made using a pure covalence at -190 ppm and a weakened covalence at -170 ppm (or dilutive) components. The evolution of their relative areas is summarised in Figure 3b, where C, D and M respectively stand for Covalent, Dilutive and Massif. The semi-covalent component dominates, except for the highest fluorination temperature, where the covalent bonds are

slightly predominant. It can be seen on Figure 3b that the evolution of the components does not seem to be linked to the temperature evolution.

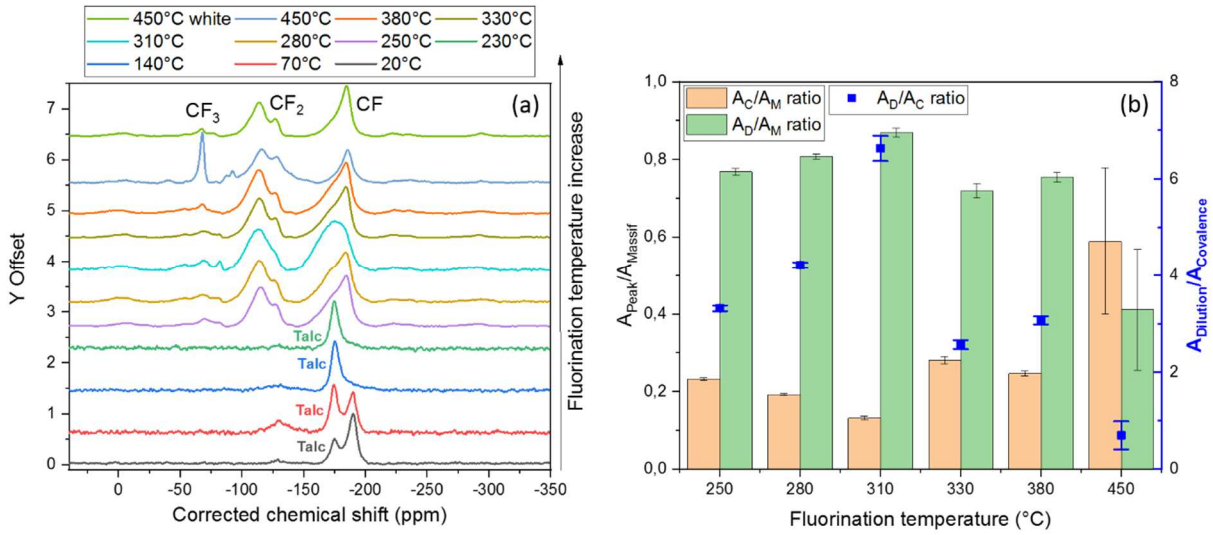

Figure 3: (a) Normalised ^{19}F NMR spectra of FCF samples, (b) evolution of the ^{19}F NMR CF peak relative areas depending on the fluorination temperature *[print with colour]*

The last analysis carried out to follow the structural evolutions is EPR. This technique allows to follow another defects, i.e. the dangling bonds of fluorinated fibres and sizing (Figure 4a). Sized Non-F fibres exhibit the highest number of dangling bonds. These bonds do not come from the sizing, as shown in Figure 4b: the high signal-to-noise ratios and the weak signal intensities for both Non-F and fluorinated sizing suggest that dangling bonds are rather located in the carbon lattice and/or in the external amorphous carbon layers. According to Figure 4a, low-temperature fluorinations (FCF-20 and FCF-70 samples) drastically decrease the spin density, thus suggesting that the defects in the external carbon layers are eliminated even at these temperatures. If this observation is correlated to the increase of the coherence length (Table 2), one may propose that the dangling bonds are located in the amorphous regions of the carbon lattice. It is known that fluorination form radicals in fluorinated polymer [15]. The high spin density of FCF-140 sample could be explained by the decomposition of the sizing, and C-C and C-H bond cleavage. It must be noted that this sample exhibit one band at 1750 cm^{-1} in the IR spectrum (Figure 1a). Its assignment for fluorinated polymers is C=O due to the post-reactivity during the exposure in air after fluorination and the reaction of radicals with O_2 or H_2O. Some of the radicals were not accessible for oxygen and H_2O or stabilised by fluorine environment. The high spin density in fluorinated sizing appears as an indirect evidence of the sizing decomposition, strengthening the previous hypotheses.

When the sizing is fully removed, the changes in spin density are more easily interpretable. FCF-230 sample has a weak spin density, showing that fibres have been purified from both their sizing and their external amorphous layers, as evidenced through ATR-FTIR and ^{19}F NMR. Higher fluorination temperatures lead to the formation of dangling bonds, located in the fluorinated phase, with a maximal spin density reached for FCF-330 sample. The decrease of spin density for FCF-380 sample is another evidence of the departure of the fluorinated phase at this temperature.

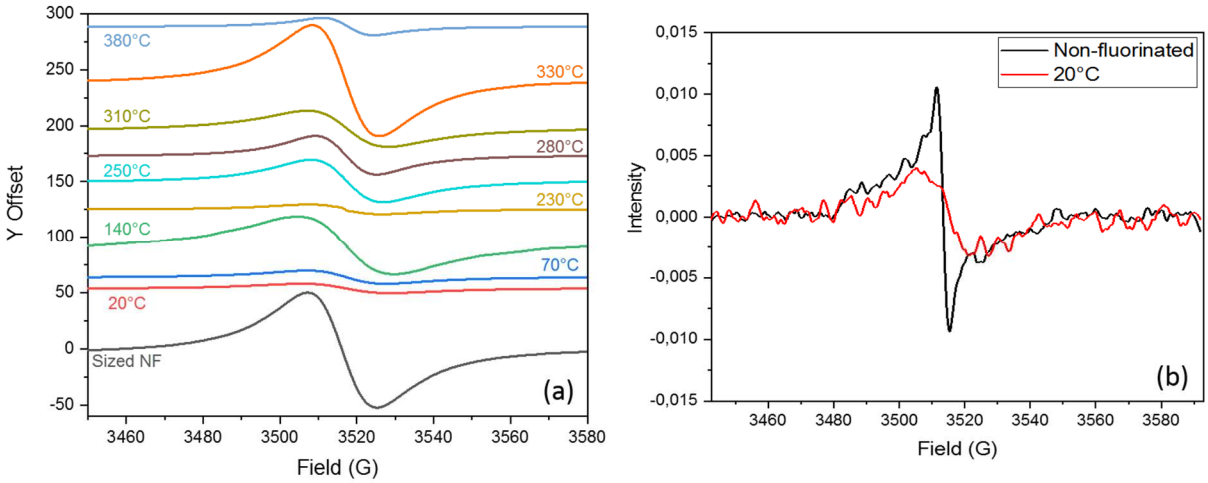

Figure 4: EPR spectra of (a) fluorinated carbon fibres, (b) Non-F and fluorinated sizing *[print with colour]*

The non-monotonous changes of the spin density need the cross-checking of data from different techniques (FTIR, Raman, SEM, and AFM, the last two being discussed thereafter) to be fully understood. To sum up the input of EPR data, low-temperature fluorination acts as a purification step by eliminating both the sizing and amorphous carbon layers, the latter ones being rich in dangling bonds; a decrease of the spin density is observed. At 230°C, the fibre is cleaned but not significantly fluorinated yet, resulting in a minimal spin density. Higher fluorination temperatures, up to 330°C, lead to the formation of dangling bonds as seen for other carbonaceous materials at higher temperatures [59,60]. At 380°C, the departure of the fluorinated phase results in the decrease of the spin density, because the dangling bonds are located in this phase.

All along this section dedicated to the structural modifications brought by fluorination, two fluorination routes were evidenced, with 230°C being the transition temperature between them. Under a well-chosen temperature, fluorination thus appears as a dry process to clean the fibre surface from the sizing, without fluorinating the fibre. Usual desizing treatments are wet processes implying acetone [16,19,23], which completely disqualify them for further

integration of fibres as composite reinforcement, as wet processes may dismantle the carbon fabric structure. Rather than this desizing method, fluorination has been considered as an in situ desizing method, thanks to the difference of reactivity between fibres and sizing.

Under 230°C, the sizing is progressively fluorinated, perfluorinated and overfluorinated with the temperature increase, until it is completely eliminated at 230°C. Carbon fibre fluorination takes place from 250°C, with formation of a $(CF)_n$ pattern and an organised structure, the latter one being progressively degraded by the temperature increase. This increase leads to both an increase of the covalence of the CF bonds and to overfluorination mechanisms through the emission of gaseous fluorides. Next sections aim to strengthen these conclusions through the study of surface fluorine content and fluorinated fibre properties.

3.3 Surface fluorine content

In this section, the way fluorine atoms graft into the carbon fibre will be studied. SEM images of the fluorinated fibres are gathered in Figure 5. The FCF-140 sample appears smooth, but small bulges can be observed on its surface. These irregularities could be remaining sizing traces: as it has been shown that a room-temperature fluorination for 30 minutes already degrades sizing [25], and as fluorination is a thermally activated reaction [17,27], fluorination at 140°C for 20 minutes could also lead to sizing degradation. On the other hand, FCF-230 and FCF-250 samples look perfectly smooth with no irregularities, suggesting the completion of the sizing decomposition under F_2, already evidenced in previous sections.

The last image shows a fibre treated at 380°C, which has been attacked and degraded by fluorine, leading to the formation of holes [16]. The outer layers of the fibre seem to have become porous, as already observed in [34], and much rougher than the Non-F sized fibres. This degradation comes from both exfoliation, highlighted in the XRD analysis, and decomposition of less ordered parts; the exfoliation is favoured by both a high temperature [61] and a high F_2 flow (close to 200 mL/min), fluorination reactions being highly exothermic. Moreover, the exfoliation results in new surface that locally increases the temperature via this exothermicity [62]. All these observations match with the conclusions of section 3.2.

The porous outer layers of FCF-380 sample suggest that two phases may coexist in this fluorinated fibre: the fluorinated external layers, and the Non-F fibre bulk, leading to a core-shell structure, already found in [63] on carbon nanomaterials. As highlighted by Figure SI 6, a similar assumption can be made on FCF-250 sample: Figure SI 6a reveals the core of a

metallised fibre, by pull-out of a fragment of the fluorinated shell, and Figure SI 6b shows the etching of the fibre shell by the moving electron beam if the fibre is not metallised, exposing the fibre core. Moreover, this need to metallise high-temperature fluorinated fibres evidences a conductivity loss, highlighting covalent bonding [26].

Figure 5e gathers EDX analyses of the shells and cores of fluorinated fibres. Until 70°C, the major fluorination reaction seems to affect the sizing, as the fluorine rate slightly increases; since the sizing is only 0.5-2 wt% of the {fibre + sizing} system [64], the fluorine content is low. At 140°C, the fluorine atomic percentage decreases, evidencing an overfluorination and a degradation of the sizing (Figure 5b). At 230°C, given the low fluorine rate, the removal of the fluorinated sizing is almost complete, but the fibre is not fluorinated yet, in good agreement with the previous sections. The carbon fibre fluorination starts at 250°C, and high amounts of fluorine are grafted above 280°C. The temperature appears to be a crucial factor to reach high rates of grafted fluorine. Fluorine is more abundant on the fibre shell surface than on the fibre core one.

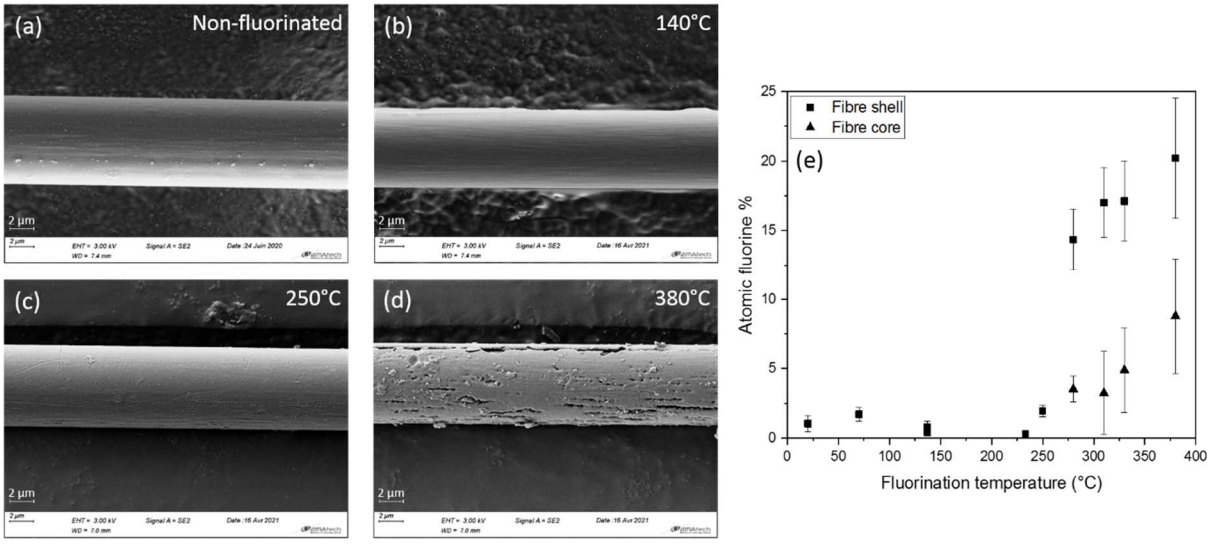

Figure 5: SEM images of (a) Sized Non-F carbon fibres, (b) FCF-140, (c) FCF-250, (d) FCF-380 samples, and (e) surface fluorine atomic percentage depending on fluorination temperature using EDX

Fibre diameters measured on SEM images are reported in Table 3. From 140°C to 230°C, the fibre diameter decreases. Knowing that the sizing thickness is 0.1-1 µm, temperature increase up to 230°C highlights a progressive sizing fluorination and elimination. At 250°C, the diameter increases, which could be due to a swelling of the fibre by fluorine penetrating into it. For higher temperatures, the diameter decrease could be explained by carbon fibre degradation by fluorine, leading to the emission of gaseous carbon fluorides.

Table 3: Fibre diameter depending on the fluorination temperature

Fluorination temp. (°C)	Non-F	20	140	230	250	380
Average diameter (µm)	7.13 ± 0.04	7.12 ± 0.07	6.50 ± 0.08	6.36 ± 0.05	6.76 ± 0.06	6.4 ± 0.1
Loss %	0	0.08	8.8	10.8	5.1	9.6

EDX analyses have also been carried out on fibre transversal sections, in order to study fluorine diffusion into the fibre bulk, as shown in Table 4 and Figure 6. The fluorine relative contents follow the same trend than in Figure 5e, but are lower in accordance with the analysis depth of EDX (1-3 µm); EDX analyses of Figure 5e mainly detect the fluorine of the shell highlighted in Figure SI 6, while EDX analyses of Table 4 and Figure 6 are more focused on the fibre core. The cartographies shown in Figure 6 confirm the hypothesis of fluorinated layers surrounding a less or not fluorinated core. The depth of the fluorinated shell and its fluorine content appear to be more important for FCF-380 sample (1.4 nm) than for FCF-250 sample (1.0 nm). Lastly, the high proportion of nitrogen detected for Sized Non-F fibres could be imputed to a potential fibre treatment before sizing, such as nitric acid oxidation. These atoms are not present anymore for the fluorinated fibre because of the reaction given thereafter, which converts nitrogen atoms from solid to gaseous state.

$$C - N + 2\,F_2 \rightarrow NF_3\,(g) + C - F$$

Traces of Al and Mg detected post-fluorination could be due to a pollution of the fluorination reactor.

Table 4: Fluorine atomic % on transversal section of fibre depending on fluorination temperature using EDX

Fluorination temperature (°C)	Sized Non-F	250	380
C	93.0 ± 0.3	91.0 ± 0.2	84.8 ± 0.2
F		4.6 ± 0.1	10.4 ± 0.2
O	1.1 ± 0.1	4.5 ± 0.2	3.8 ± 0.2
N	5.3 ± 0.3	-	-
Al, Mg	-	-	2.1 ± 0.1

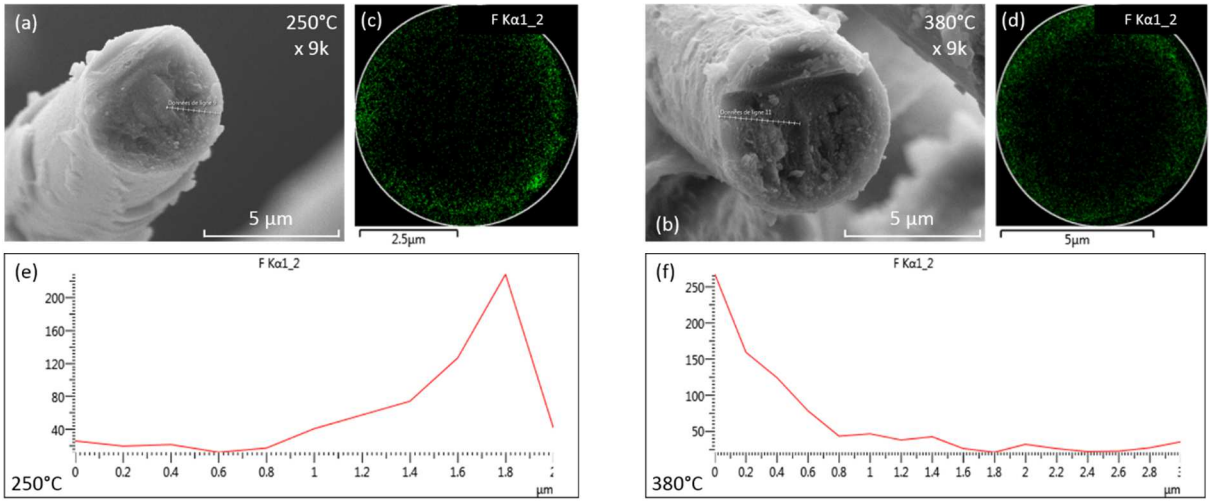

Figure 6: Transversal sections of (a) FCF-250, (b) FCF-380 samples, correlated with their respective EDX fluorine repartition ((c) and (d)) and fluorine diffusion depths ((e) and (f))

SEM and EDX analyses have evidenced the hypothesis of an external fluorinated layer coating a less or not fluorinated bulk; both the fluorine content and the depth of the fluorinated layer increase with the reaction temperature. The conclusions of section 3.2 are strengthened by these observations.

XPS analyses were carried out because the fluorine grafting appears to be mainly on the fibre surface. XPS data have been gathered in Table SI 3. Concerning the Non-F fibres, as the spectra of desized and sized ones were collected with and without flood gun, as shown in Figure SI 7, it has been possible to highlight the shift of some peaks to high binding energies, confirming the presence of the sizing on both the sized fibres and the chemically desized ones. Weak shifts for the latter ones underline a low remaining sizing quantity. Moreover, according to Table SI 3, CO bonds are mostly C-O-C for sized fibres, as there are twice more CO bonds in C 1s peak (33%) than in O 1s peak (18%), which could indicate the DGEBA epoxy groups. On the other hand, for desized fibres, the proportions of CO in C 1s and O 1s peaks are similar, which confirms the sizing disappearance; the detected oxygen atoms are probably the ones of C-OH groups of the fibres with some C-O-C from the residual sizing. The shift of small peaks to higher binding energies confirms the presence of sizing traces.

Fluorination of unsized graphitic carbon fibres creates two types (I and II) of C-F bonds [62,65], which are distinguishable in XPS using the flood gun. Type I belongs to weakly fluorinated areas and its environment is similar to the carbon sp^2 one (C-F bonds with weakened covalence). Its binding energy is steady, independently of the electron flow. The binding energy of type II is adjustable with the flood gun, as it undergoes a charging effect

because of the insulating properties of the area (covalent C-F bonding) [66], meaning that type II C 1s and F 1s binding energies tend to be higher than type I ones [67].

Concerning sized fibres, whose XPS C 1s spectra are given in Figure 7, if fluorination occurs on carbon fibres and not on DGEBA, the CF peak is noted type I and has to be greater than the CF_2 and CF_3 ones [65]. However, fibres fluorinated at low temperatures (FCF-20 and FCF-140 samples) exhibit higher CF_2 and CF_3 peaks than the type I C-F peak, evidencing that the fluorination only occurs on the sizing, as already highlighted by ATR-FTIR analyses. It should also be noted that the proportion of fluorinated species is similar for FCF-20 and FCF-140 samples, meaning that the temperature increase, which is a favourable factor for further fluorination [37], is offset by the sizing degradation, which eliminates fluorinated species from the fibre surface. However, as stated in the Comments section of Table SI 3, the CF_2 relative content is almost twice higher in FCF-140 sample (11.7%) than in FCF-20 sample (6.3%), which proves the increasing intensity of the fluorination rate with temperature, as already seen for polymers [14,15,39,68,69], and taking into account the ^{19}F NMR analyses.

Fibres fluorinated at higher temperatures (FCF-250, FCF-380 and FCF-450 samples) become completely insulating on their surface because of the sp^2 into sp^3 hybridization conversion and formation of type II CF bonds. Moreover, the high binding energies of C-F bonds, observable in Table SI 3 and Figure 7, highlight type II bonding (fluorinated graphite) and a $(CF)_n$ structure, already evidenced through XRD. The detected CF_2 bonds probably come from the edges. Lastly, oxygen has disappeared, confirming the completion of sizing decomposition observed in ATR-FTIR from 230°C.

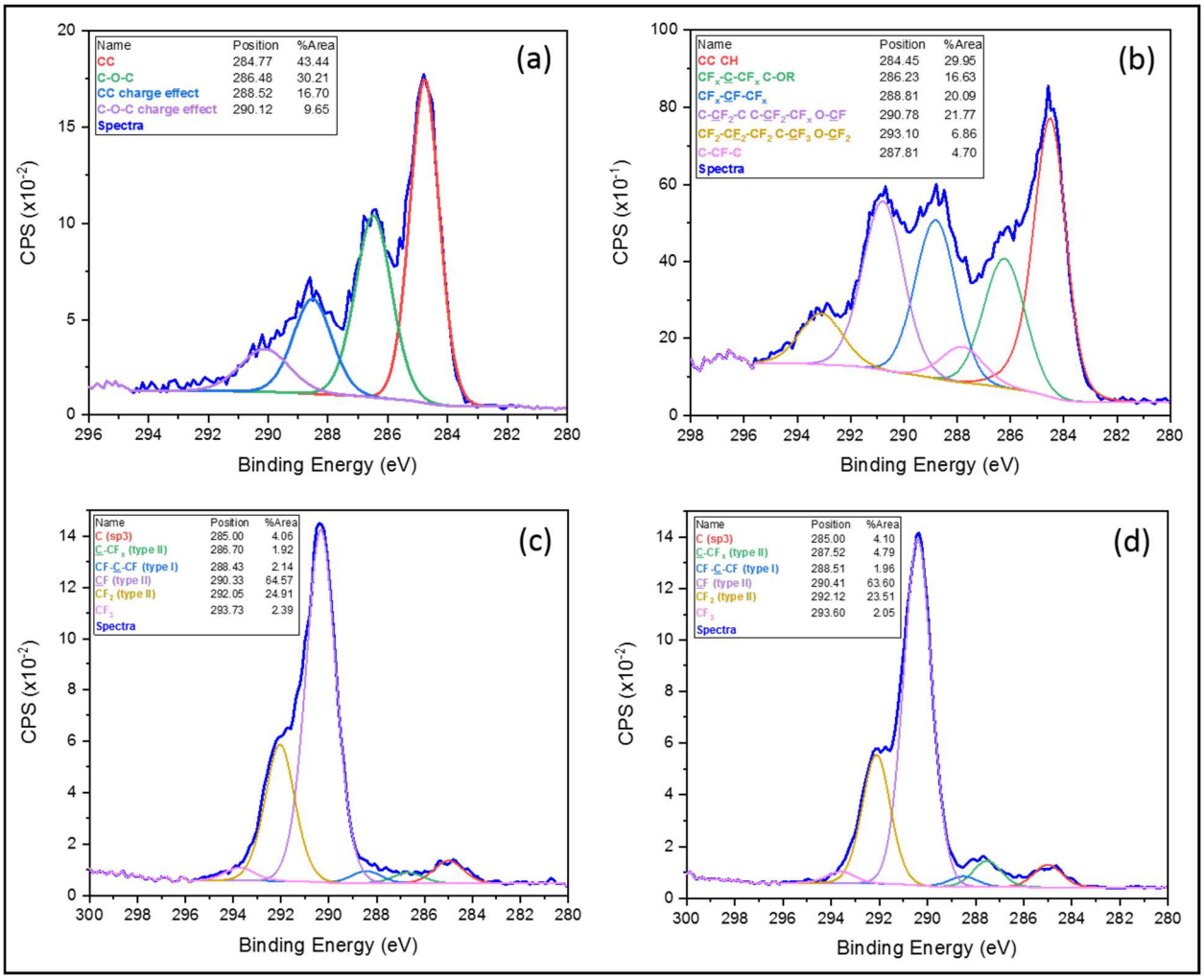

Figure 7: XPS C 1s spectra of (a) Non-F sized (flood off), (b) FCF-140, (c) FCF-250, (d) FCF-380 samples *[print with colour]*

In order to compare surface and bulk fluorination phenomena, the integrated areas *S* of CF, CF_2 and CF_3 groups were calculated for both ^{19}F NMR (representative of the fibre bulk, bulk meaning here the fluorinated layer and not the core of the fibre, not reached by fluorination in these conditions) and XPS (representative of the fibre outmost surface) and are gathered in Table 5. Considering the S_{CF3}/S_{CF2} and S_{CF3}/S_{CF} ratios, it can be seen that they both increase with temperature according to ^{19}F NMR analyses, while XPS analyses rather evidence a decrease. This could highlight a progressive increase of CF_3 groups in the fibre bulk, while these groups are eliminated at the outmost surface of the fibre through the formation of gaseous fluorides. Such an observation is in accordance with the diffusion limited character of gas/solid fluorination. The bulk is perfluorinated and overfluorinated after the surface. The increase of the bulk (^{19}F NMR data) S_{CF2}/S_{CF} ratio while the surface (XPS) one remains constant also highlights a progressive perfluorination of the fibre bulk, while the outer surface

is already perfluorinated. The fluorination is limited by the diffusion as for the case of polymers [15].

Table 5: Comparison of relative area ratios depending on the fluorination temperature and the used analysis

	S_{CF3}/S_{CF2}		S_{CF3}/S_{CF}		S_{CF2}/S_{CF}	
Fluorination temperature (°C)	^{19}F NMR	XPS	^{19}F NMR	XPS	^{19}F NMR	XPS
250	0.05	0.10	0.04	0.037	0.8	0.39
380	0.09	0.09	0.08	0.032	1.0	0.37
450	0.14	0.07	0.40	0.025	2.8	0.38

In this part, the surface fluorine content and the way fluorine grafts to the carbon fibres depending on the fluorination temperature have both been investigated using SEM-EDX and XPS analysis. All the observations match with the hypotheses of section 3.2. It can be added that for high-temperature fluorinations, a core-shell structure is created with the shell depth increasing with fluorination temperature. XPS analyses highlighted a covalent (type II) C-F bonding, meaning that fluorination has replaced in large regions the sp^2 graphitic configuration by fluorinated graphite with a $(C_2F)_n$ or $(CF)_n$ structure. Such type II C-F make the fibre insulating, as seen through XPS analysis and the need to metallise the fibres to avoid their etching by the SEM electron flow. The influence of these modifications on the surface properties of carbon fibres will be discussed thereafter.

3.4 Fluorination impact on surface properties

3.4.1 Wettability and surface energy

Contact angles were measured using two different reference liquids, which enables the polar and dispersive parts of the surface energy to be determined [25], thanks to the Owens and Wendt's equations [70,71]. The polar and dispersive components of fluorinated carbon fibres, obtained by both the sessile drop method and the tensiometric one, are given in Figure 8. Fluorination drastically reduces the total surface energy, as the energies of fluorinated fibres are at least divided by 2 when compared to the Non-F sized and desized fibres. The fact that FCF-230 sample has the highest surface energy of fluorinated fibres can be linked to the absence of fluorine at the fibre surface due to the complete desizing of the fibre without fluorination of the carbonaceous material, as seen through all the previous analyses.

Higher fluorination temperatures result in a decrease of the surface energy, and especially its polar component, with a minimum reached for FCF-330 sample. The further increase of surface energy for FCF-380 and FCF-450 samples is due to the increase of the dispersive component, which appears to be sensitive to surface morphology. This hypothesis is strengthened by the surface aspect of FCF-380 sample, which is highly different from the other samples, as highlighted in Figure 5d. As already stated, this aspect is mainly due to the exfoliation caused by both high fluorine flow and high temperature.

The comparison of the surface energies obtained with the drop method and the tensiometric one highlights that, although the values are quite different (10 $mN.m^{-1}$ against 24 $mN.m^{-1}$ and 3 $mN.m^{-1}$ against 15 $mN.m^{-1}$ for FCF-250 and FCF-330 samples respectively), the general trend is similar: presence of F atoms greatly decreases the surface energy, especially its polar component, temperature being an activator of this decrease.

As fluorination decreases the polar component of surface energy, the fibres become more hydrophobic, as shown in Figure 8. The highest contact angles, above 130°, are reached for high-temperature fluorinated fibres, where the fluorine atoms have been covalently grafted to the carbon lattice, this effect being strengthened by the carbon fibre debundling that occurs from 230°C, potentially introducing a different morphological effect than for fibres fluorinated below this temperature. The lowest contact angle is measured for FCF-140 sample, due to its important polar component leading to higher affinity with water, which has already been evidenced in ATR-FTIR through the 1750 cm^{-1} band attributed to -COOH groups.

The interest of the fluorination treatment is to decrease the high polar component of non-fluorinated fibres measured through tensiometric method, in order to reduce the gap between this component and the polar one of the epoxy resin, as it has been established that more hydrophobic fibres could be better impregnated by hydrophobic resins [72], and that close polar and dispersive components between fibres and matrix could lead to a better fibre/matrix interface [38].

This outlines the possibility to tailor the surface energy components of carbon fibres to enhance their compatibility with other polymer matrices, such as polyethylene or polypropylene. Fluorination thus appears as a way to custom the fibre surface energy depending on a given matrix, while sizing and coupling agents predestine the use of a particular matrix, which has to be adapted to the sizing.

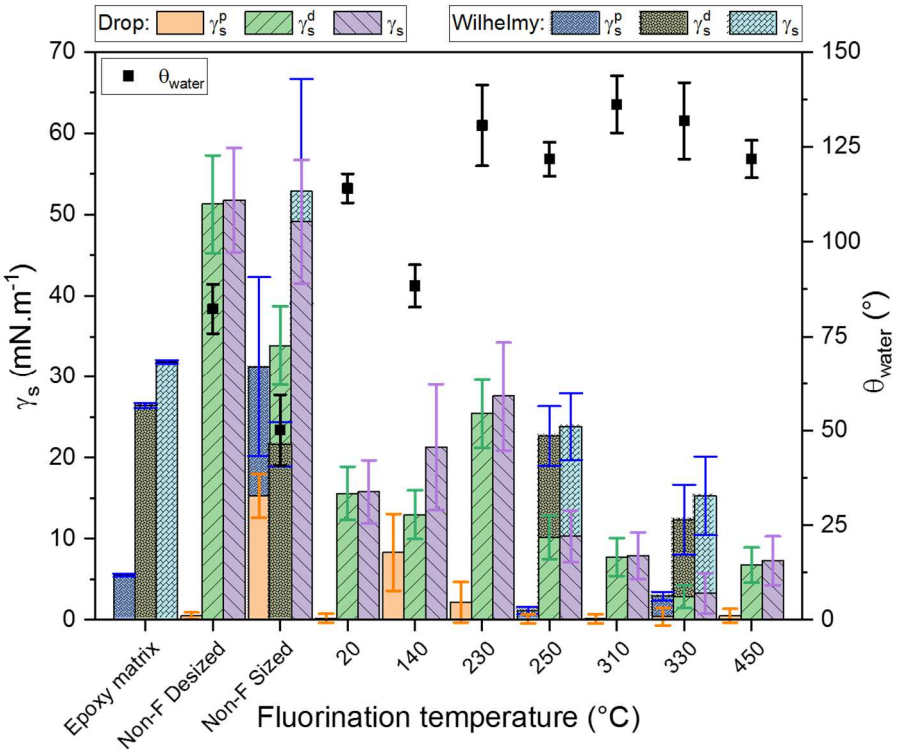

Figure 8: Dispersive and polar components (tensiometric and drop methods) and contact angles with water of carbon fibres depending on fluorination temperature *[print with colour]*

3.4.2 Surface morphology

In order to investigate the surface morphology of Non-F and fluorinated fibres, topography and phase images were acquired using AFM and are respectively gathered in Figure 9 and Figure SI 8. Both images reveal that the smoothest fibre amongst the analysed samples is the Non-F sized one. Small bumps are visible at the surface of FCF-250 sample, which looked smooth in Figure 5c. These bumps could result either from a slight etching of the fibre by fluorine or from fluorine penetration into the fibre bulk, leading to fibre swelling, as already seen on carbonaceous materials [73,74].

The small irregularities observable at the surface of the FCF-380 sample are coherent with its SEM image in Figure 5d. Moreover, its phase image (Figure SI 8) highlights the apparition of a roughening at the nanometric scale that results from both the etching and exfoliation of the fibre by fluorine gas, as seen in Figure 5. Based on Wenzel model, this roughening at the nanometric scale can explain the increase of the dispersive component in Figure 8.

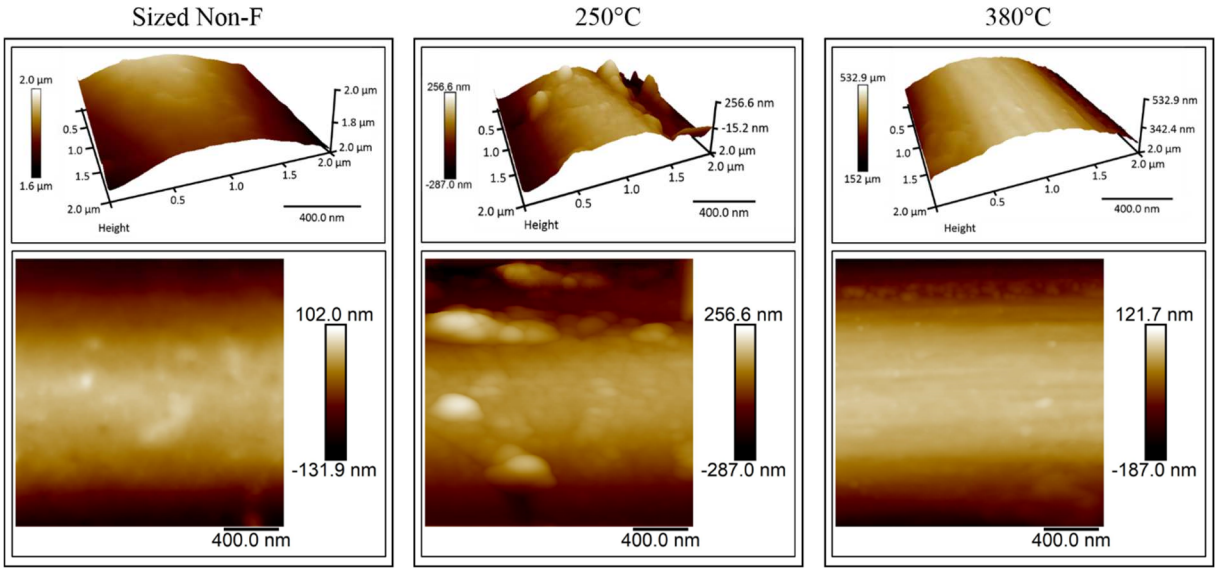

Figure 9: AFM topography images of carbon fibres depending on fluorination temperature

In this section, the surface properties of fluorinated carbon fibres have been investigated. It has been evidenced that fluorination strongly reduces the surface energy of carbon fibres, especially its polar component, which leads to a huge increase of contact angle with water. AFM analyses have highlighted the etching and partial exfoliation of carbon fibres by fluorine with the creation of a roughening at the nanometric scale. These irregularities may lead to an improvement of the fibre-matrix adhesion in composite materials by mechanical interlocking. On the other hand, fluorination has only a tiny influence on friction coefficients. The latter ones are increasing with high fluorine proportions or with the presence of fluorinated sizing, while low fluorine proportions or fibre desizing tend to decrease them.

3.5 Fluorination impact on mechanical properties

The mechanical properties of fluorinated carbon fibres have been investigated through tensile tests, whose results have been gathered in Table 6. High fluorination temperatures (≥ 330°C) lead to low Weibull moduli [19,34], highlighting a loss of reliability on the tensile properties, as these moduli can be considered as flaw frequency distribution factors [75]. Tensile strength also decreases, underlining a surface degradation, as tensile strength is related to the fibre surface state [38]. Moreover, Young's moduli, which are rather reflecting volume properties [38] of the fibres, are also decreasing at these fluorination temperatures, highlighting the severe degradation induced by high-temperature fluorinations. Even FCF-280 and FCF-310 samples have relatively low moduli, showing a slight fibre weakening.

On the other hand, treatments at low fluorination temperature (< 230°C) barely modify the tensile properties of carbon fibres, although the mechanical properties slightly decrease with the temperature increase (140°C and 230°C). This highlights the small influence of fluorination on the fibre at these temperatures and the fact that only the sizing is affected, as previously stated.

Lastly, regarding its stress at strain and Young's modulus, FCF-250 sample appears to be the strongest one, even more than the Non-F fibres. Moreover, it seems to be much more reliable than the other fibres, treated or not, thanks to its relatively high Weibull modulus, even compared to carbon fibre moduli at similar gauge lengths in literature [76]. According to mechanical properties, 250°C thus appears to be the optimal fluorination temperature; this fibre reinforcement and reliability increase, coupled with the fibre purification highlighted through SEM, ATR-FTIR and EPR observations, may lead to describe fluorination at this temperature as a healing process for the fibre. It should however be noted that this temperature depends on each sizing/fibre couple, and that this treatment may not be universal and must be tailored for every carbon fibre, *e.g.* depending on its precursor.

This healing effect was unexpected, because literature mainly reports a conservation or a decrease of Weibull and Young moduli and of tensile stress at break [16,19,34]. Mechanical improvements may however be obtained under oxyfluorination or F_2-HF fluorination conditions, with low concentrations of fluorine into the fibres in the latter case [27,74].

Moreover, to ensure that the mechanical improvement of FCF-250 sample is related to the fluorine grafting and not only to the temperature increase, carbon fibres were heated at 250°C for 20 min into a N_2 atmosphere. Their mechanical properties are given in Table 6 (sample "250-N_2"), and are similar to the Non-F fibre ones, highlighting the fluorine effect in the improvement of carbon fibre mechanical properties.

Table 6: Mechanical properties of fluorinated carbon fibres

Fluorination temp. (°C)	Desized Non-F	Sized Non-F	20	140	230	250	250-N_2	280	310	330	380
Young's modulus (GPa)	220 ± 20	200 ± 20	220 ± 20	190 ± 30	180 ± 30	210 ± 10	220 ± 20	170 ± 20	170 ± 30	120 ± 40	130 ± 40
Stress at break (MPa)	4200 ± 900	4000 ± 900	4000 ± 900	3900 ± 1100	3300 ± 1100	5000 ± 900	4300 ± 1000	3700 ± 1000	4000 ± 1000	2900 ± 1200	3600 ± 1000
Strain at break (%)	1.6 ± 0.4	1.7 ± 0.4	1.5 ± 0.3	1.7 ± 0.5	1.7 ± 0.6	1.9 ± 0.3	-	1.8 ± 0.4	2.0 ± 0.6	2.2 ± 1.1	2.5 ± 1.1
Weibull modulus	4.7	4.3	5.1	3.5	3.0	8.6	4.1	3.6	3.8	2.3	4.1

σ_0 (MPa)	4600	4440	4360	4340	3750	5460	4800	4100	4410	3290	4020
R^2	0.99	0.96	0.98	0.98	0.98	0.96	0.99	0.98	0.97	1.00	0.97
ATR-IR massif area	-	-	-	-	-	2.5	-	3.4	5.0	11.8	4.3

The Weibull moduli appear to be conversely related with the area of the ATR-FTIR massif of superimposed C-F bands, as shown in Table 6. This means that the more fluorine atoms are grafted to the fibres, the less the fibres are mechanically reliable. Once again, the interest of a weak carbon fluorination is pointed out, while heavier fluorine grating only leads to poor mechanical properties, which does not seem relevant for further use in composite materials as reinforcing fibres.

3.6 Thermal degradation of fluorinated carbon fibres (TGA-MS)

Thermo-Gravimetric Analyses (TGA) were carried out on fluorinated fibres and on sizing, as reported in Figure 10 and Figure SI 9. The chosen line types of Figure 10a evidence the difference of behaviour between low-temperature fluorinated carbon fibres and high-temperature ones. The first ones lose a little weight (up to 8%), which can be mostly attributed to the sizing thermal degradation, as shown by Figure SI 9, and to the removal of disorganised and fluorinated external layers of the fibres. Moreover, FCF-230 sample, which is fully desized according to the previous analyses, is almost thermally stable, underlining the stability of carbon and the sensitivity of the sizing at these temperatures.

The weight losses of high-temperature fluorinated fibres are high because of the decomposition of fluorinated groups. In order to know which gases have been released, TGA-MS has been carried out (Figure 10b). It has been shown by TGA measurement on FCF-230 sample, which is completely desized, that the carbon fibre was barely affected by the temperature increase, meaning that the gases detected through mass spectrometry for the Non-F sized fibres might only come from the sizing thermal decomposition. The main species observed, already seen for DGEBA TGA-MS under inert atmosphere [77], are CO_2 (m/z = 44) and unsaturated aliphatic hydrocarbons (CH_2 in this case, m/z = 14), the latter ones also potentially coming from defect sites and layer edges of the graphitic phase of the carbon fibre. The m/z ratio of 14 could also be linked to N from N_2, while m/z = 28 could be attributed both to CO, coming from the cracking pattern of CO_2, and to N_2 molecules adsorbed during air exposure previously to the TGA-MS measurements. Lastly, the m/z ratio of 32 could come

from O_2, both from the sizing thermal degradation and to O_2 molecules adsorbed previously to the TGA-MS measurements.

Concerning the fluorinated fibres, the predominant peak is the fluorine one (*m/z* = 19), which may come from intercalated fluorine semi-covalently linked to the sp^2 structure and de-intercalated by the temperature increase. When compared to Non-F sized fibres, some peaks are less intense: the CH_2 peak (*m/z* = 14) is reduced, especially for FCF-380 sample, because of the sizing overfluorination and of the hydrogen replacement by fluorine for the CH_2 groups. Moreover, if this peak was due to N atoms coming from the Non-F sized fibre, the latter ones are consumed by the reaction given in section 3.3, which can also explain the decrease of this peak.

Concerning the emerging peaks, three of them (*m/z* = 31, 50, 69) can be linked to fluorine grafting, are they respectively represent CF, CF_2 and CF_3 groups, which have already been observed for thermal degradation of $(CF)_n$ [78].

As fluorine appears to be the most detected species for fluorinated fibres, the bulk F/C ratio of each fibre has been determined in Table 7, where the onset temperatures of degradation have also been gathered. The fibres fluorinated above 250°C have much higher ratios than the ones fluorinated under 230°C, as not only the sizing has been fluorinated. FCF-450 sample has an extremely low ratio, underlining potential overfluorination and fluorine departure during the fluorination treatment.

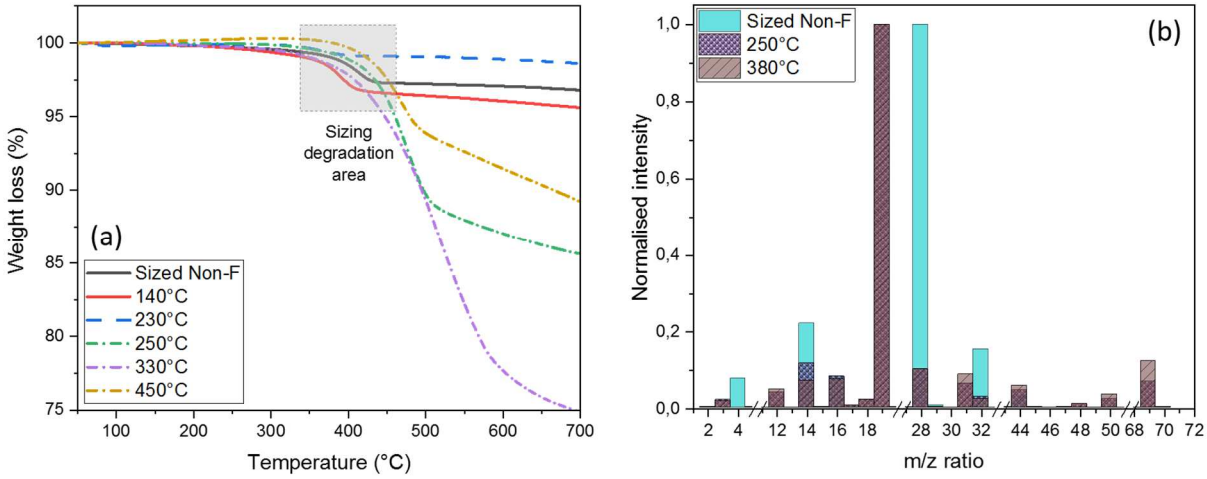

Figure 10: (a) TGA of fluorinated carbon fibres, (b) MS of Sized Non-F fibres, FCF-250 and FCF-380 samples *[print with colour]*

Table 7: Bulk F/C ratios and degradation temperatures of fluorinated carbon fibres

Fluorination temperature (°C)	Sized Non-F	20	70	140	230	250	280	310	330	380	450
F/C ratio (10^{-2})	-	3.4	2.3	2.1	0.6	7.9	16.4	9.1	18.2	30.8	3.9
Degradation temperature (°C)	370	390	380	350	320	420	440	460	430	430	410

4 Conclusions

Direct fluorination with diluted F_2 gas (with N_2) was applied to DGEBA-sized carbon fibres at various temperatures (from RT to 450°C) for 20 minutes. Depending on the fluorination temperature, several fluorination routes have been identified. First, RT fluorination leads to the sizing fluorination, as already described in [25]. From 140°C to 230°C, the sizing is first perfluorinated and then degraded through overfluorination reactions with fluorinated sizing traces remaining at the fibre surface, while the carbonaceous lattice of the fibres is not fluorinated yet. The progressive degradation of the fluorinated sizing leads to an increase of the surface energy, which is maximal at 230°C. From 250°C to 330°C, the carbon fibre fluorination occurs with an increasing fluorine quantity. A core-shell structure arises, with higher surface fluorine content for shell than for core, and an increase of the shell fluorine concentration and depth with temperature. The resulting C-F bonding is covalent, evidencing that the fluorination has replaced the sp^2 graphitic configuration by fluorinated graphite with a $(CF)_n$ structure, which increases the coherence length of the graphitic phase by removing most of the amorphous carbons. Thanks to the increasing covalence of fluorinated bonds with temperature, fluorine grafting leads to a hydrophobicity enhancement. A progressive perfluorination of the fibre bulk with temperature, while the outer surface is readily perfluorinated, has also been evidenced.

The optimum temperature appears to be 250°C, as the tensile properties are remarkably better and more reliable than for other fluorinated fibres. The interest of a slight carbon fluorination for further use in composite materials is thus pointed out. Moreover, slight etching and potential swelling of the fibre both create irregularities; such a morphology may favour the fibre-matrix adhesion in composites.

Above 380°C, fluorine strongly degrades the carbon lattice through exfoliation and overfluorination phenomena. Degradation is evidenced through the increase of I_D/I_G ratio and the decrease of the coherence length. CF_3 groups and gaseous fluorides are formed via C-C bond cleavage, which result in the formation of dangling bonds.

Further use of fibres fluorinated under the optimum fluorination conditions as reinforcing fibres in composite materials is the next step of the present investigations. A better resistance to wet ageing is expected from the composites reinforced with fluorinated carbon fibres, thanks to their hydrophobicity. If stronger fibre/matrix interface adhesion and acceptable mechanical properties are also obtained, fluorination could be considered as a serious candidate to compete with sizing treatments their functionalising role, fluorination having the advantage to be a dry process and to allow a tailoring of the fibre surface energy, avoiding to predestine fibres to be used with a specific matrix depending on the chosen coupling agent.

Acknowledgements

The authors thank the Inorganic Material team of the Institut de Chimie de Clermont-Ferrand for their help during the experimental phase. The authors also thank M. F. Pucci (Laboratoire de Mécanique et Génie Civil, France) and P.-J. Liotier (Polymères Composites Hybrides, France) for their help and fruitful discussion on wettability measurements. This work was supported by SIGMA Clermont.

References

[1] S. Tiwari, J. Bijwe, Surface Treatment of Carbon Fibers - A Review, Procedia Technol. 14 (2014) 505–512. https://doi.org/10.1016/j.protcy.2014.08.064.

[2] L.T. Drzal, The interphase in epoxy composites, in: K. Dušek (Ed.), Epoxy Resins and Composites II, Springer-Verlag, 1986: pp. 1–32. https://doi.org/10.1007/BFb0017913.

[3] S. Chand, Review Carbon fibers for composites, J. Mater. Sci. 35 (2000) 1303–1313. https://doi.org/10.1023/A:1004780301489.

[4] M. Tourlonias, M.-A. Bueno, C. Jordan, D. Poquillon, Influence of Wear on the Sizing Layer and Desizing of Single Carbon Fibre-to-Fibre Friction, Wear. 402–403 (2018) 64–70. https://doi.org/10.1016/j.wear.2018.02.003.

[5] J.D.H. Hughes, The carbon fibre/epoxy interface - A review, Compos Sci Technol. 41 (1991) 13–45. https://doi.org/10.1016/0266-3538(91)90050-Y.

[6] F.R. Jones, A Review of Interphase Formation and Design in Fibre-Reinforced Composites, J Adhes Sci Technol. 24 (2010) 171–202. https://doi.org/10.1163/016942409X12579497420609.

[7] R.L. Zhang, Y.D. Huang, L. Liu, Y.R. Tang, D. Su, L.W. Xu, Effect of emulsifier content of sizing agent on the surface of carbon fibres and interface of its composites, Appl. Surf. Sci. 257 (2011) 3519–3523. https://doi.org/10.1016/j.apsusc.2010.11.066.

[8] L.T. Drzal, M.J. Rich, M.F. Koenig, Adhesion of Graphite Fibers to Epoxy Matrices. III. The Effect of Hygrothermal Exposure, J Adhes. 18 (1985) 49–72. https://doi.org/10.1080/00218468508074936.

[9] C.L. Arnold, D.J. Eyckens, L. Servinis, M.D. Nave, H. Yin, M.K.W. Ross, J. Pinson, B. Demir, T.R. Walsh, L.C. Henderson, Simultaneously increasing the hydrophobicity and interfacial adhesion of carbon fibres: a simple pathway to install passive functionality into

composites, J. Mater. Chem. A. 7 (2019) 13483–13494. https://doi.org/10.1039/C9TA02436K.
[10] O.I. Gladunova, Yu.E. Fedorova, O.V. Astashkina, A.A. Lysenko, Composites with Hydrophobic Surfaces, Fibre Chem. 47 (2015) 317–319. https://doi.org/10.1007/s10692-016-9686-5.
[11] B. Ameduri, H. Sawada, Fluorinated Polymers: Volume 2: Applications, Royal Society of Chemistry, Cambridge, 2016. https://doi.org/10.1039/9781782629368.
[12] L.-Y. Meng, S.-J. Park, Superhydrophobic carbon-based materials: a review of synthesis, structure, and applications, Carbon Lett. 15 (2014) 89–104. https://doi.org/10.5714/CL.2014.15.2.089.
[13] J. Peyroux, M. Dubois, E. Tomasella, N. Batisse, A.P. Kharitonov, D. Flahaut, L. Romana, P. Thomas, Surface modification of low-density polyethylene packaging film via direct fluorination, Surf. Coat. Technol. 292 (2016) 144–154. https://doi.org/10.1016/j.surfcoat.2016.03.021.
[14] A.P. Kharitonov, B.A. Loginov, Direct fluorination of polymer final products: From fundamental study to practical application, Russ. J. Gen. Chem. 79 (2009) 635–641. https://doi.org/10.1134/S1070363209030451.
[15] A.P. Kharitonov, L.N. Kharitonova, Surface modification of polymers by direct fluorination: A convenient approach to improve commercial properties of polymeric articles, Pure Appl. Chem. 81 (2009) 451–471. https://doi.org/10.1351/PAC-CON-08-06-02.
[16] K.K.C. Ho, G. Beamson, G. Shia, N.V. Polyakova, A. Bismarck, Surface and bulk properties of severely fluorinated carbon fibres, J. Fluorine Chem. 128 (2007) 1359–1368. https://doi.org/10.1016/j.jfluchem.2007.06.005.
[17] A. Bismarck, R. Tahhan, J. Springer, A. Schulz, T.M. Klapötke, H. Zeil, W. Michaeli, Influence of fluorination on the properties of carbon fibres, J. Fluorine Chem. 84 (1997) 127–134. https://doi.org/10.1016/S0022-1139(97)00029-8.
[18] K.K.C. Ho, A.F. Lee, A. Bismarck, Fluorination of carbon fibres in atmospheric plasma, Carbon. 45 (2007) 775–784. https://doi.org/10.1016/j.carbon.2006.11.015.
[19] K.K.C. Ho, A.F. Lee, S. Lamoriniere, A. Bismarck, Continuous atmospheric plasma fluorination of carbon fibres, Compos. Part A Appl. Sci. Manuf. 39 (2008) 364–373. https://doi.org/10.1016/j.compositesa.2007.10.008.
[20] F. Saulnier, M. Dubois, K. Charlet, L. Frezet, A. Beakou, Direct fluorination applied to wood flour used as a reinforcement for polymers, Carbohydr. Polym. 94 (2013) 642–646. https://doi.org/10.1016/j.carbpol.2013.01.060.
[21] M. Pouzet, M. Dubois, K. Charlet, A. Béakou, J.M. Leban, M. Baba, Fluorination renders the wood surface hydrophobic without any loss of physical and mechanical properties, Ind Crops Prod. 133 (2019) 133–141. https://doi.org/10.1016/j.indcrop.2019.02.044.
[22] M. Pouzet, M. Dubois, K. Charlet, A. Béakou, From hydrophilic to hydrophobic wood using direct fluorination: A localized treatment, C R Chim. 21 (2018) 800–807. https://doi.org/10.1016/j.crci.2018.03.009.
[23] K.K.C. Ho, G. Kalinka, M.Q. Tran, N.V. Polyakova, A. Bismarck, Fluorinated carbon fibres and their suitability as reinforcement for fluoropolymers, Compos. Sci. Technol. 67 (2007) 2699–2706. https://doi.org/10.1016/j.compscitech.2007.02.012.
[24] P.K. Mallick, Fiber-Reinforced Composites: Materials, Manufacturing, and Design, 3rd ed., CRC Press, 2007. https://doi.org/10.1201/9781420005981.
[25] J.-C. Agopian, O. Teraube, M. Dubois, K. Charlet, Fluorination of carbon fibre sizing without mechanical or chemical loss of the fibre, Appl. Surf. Sci. 534 (2020) 147647. https://doi.org/10.1016/j.apsusc.2020.147647.

[26] V. Gupta, R.B. Mathur, O.P. Bahl, A. Tressaud, S. Flandrois, Thermal stability of fluorine-intercalated carbon fibres, Synth. Met. 73 (1995) 69–75. https://doi.org/10.1016/0379-6779(95)03299-1.
[27] S.-J. Park, M.-K. Seo, Y.-S. Lee, Surface characteristics of fluorine-modified PAN-based carbon fibers, Carbon. 41 (2003) 723–730. https://doi.org/10.1016/S0008-6223(02)00384-6.
[28] S.-J. Park, M.-K. Seo, K.-Y. Rhee, Studies on mechanical interfacial properties of oxy-fluorinated carbon fibers-reinforced composites, Mater. Sci. Eng. A. 356 (2003) 219–226. https://doi.org/10.1016/S0921-5093(03)00134-5.
[29] A. Bosak, A. Dideikin, M. Dubois, O. Ivankov, E. Lychagin, A. Muzychka, G. Nekhaev, V. Nesvizhevsky, A. Nezvanov, R. Schweins, A. Strelkov, A. Vul', K. Zhernenkov, Fluorination of Diamond Nanoparticles in Slow Neutron Reflectors Does Not Destroy Their Crystalline Cores and Clustering While Decreasing Neutron Losses, Materials. 13 (2020) 3337. https://doi.org/10.3390/ma13153337.
[30] K. Guérin, J.P. Pinheiro, M. Dubois, Z. Fawal, F. Masin, R. Yazami, A. Hamwi, Synthesis and Characterization of Highly Fluorinated Graphite Containing sp^2 and sp^3 Carbon, Chem. Mater. 16 (2004) 1786–1792. https://doi.org/10.1021/cm034974c.
[31] W. Zhang, M. Dubois, K. Guérin, P. Bonnet, E. Petit, N. Delpuech, D. Albertini, F. Masin, A. Hamwi, Effect of graphitization on fluorination of carbon nanocones and nanodiscs, Carbon. 47 (2009) 2763–2775. https://doi.org/10.1016/j.carbon.2009.05.035.
[32] L.G. Bulusheva, Y.V. Fedoseeva, E. Flahaut, J. Rio, C.P. Ewels, V.O. Koroteev, G. Van Lier, D.V. Vyalikh, A.V. Okotrub, Effect of the fluorination technique on the surface-fluorination patterning of double-walled carbon nanotubes, Beilstein J. Nanotechnol. 8 (2017) 1688–1698. https://doi.org/10.3762/bjnano.8.169.
[33] V. Gupta, T. Nakajima, Y. Ohzawa, B. Žemva, A study on the formation mechanism of graphite fluorides by Raman spectroscopy, J. Fluorine Chem. 120 (2003) 143–150. https://doi.org/10.1016/S0022-1139(02)00323-8.
[34] I. Kruppke, C. Scheffler, F. Simon, R.-D. Hund, C. Cherif, Surface Treatment of Carbon Fibers by Oxy-Fluorination, Materials. 12 (2019) 18. https://doi.org/10.3390/ma12040565.
[35] N. Watanabe, Two types of graphite fluorides, (CF)n and (C2F)n, and discharge characteristics and mechanisms of electrodes of (CF)n and (C2F)n in lithium batteries, Solid State Ionics. 1 (1980) 87–110. https://doi.org/10.1016/0167-2738(80)90025-9.
[36] K. Guérin, M. Dubois, A. Houdayer, A. Hamwi, Applicative performances of fluorinated carbons through fluorination routes: A review, J. Fluorine Chem. 134 (2012) 11–17. https://doi.org/10.1016/j.jfluchem.2011.06.013.
[37] J.-C. Agopian, O. Téraube, K. Charlet, M. Dubois, A review about the fluorination and oxyfluorination of carbon fibres, J. Fluorine Chem. 251 (2021) 109887. https://doi.org/10.1016/j.jfluchem.2021.109887.
[38] O. Teraube, J.-C. Agopian, E. Petit, F. Metz, N. Batisse, K. Charlet, M. Dubois, Surface modification of sized vegetal fibers through direct fluorination for eco-composites, J. Fluorine Chem. 238 (2020) 109618. https://doi.org/10.1016/j.jfluchem.2020.109618.
[39] A.P. Kharitonov, Practical applications of the direct fluorination of polymers, J. Fluorine Chem. 103 (2000) 123–127. https://doi.org/10.1016/S0022-1139(99)00312-7.
[40] Z. Dai, F. Shi, B. Zhang, M. Li, Z. Zhang, Effect of sizing on carbon fiber surface properties and fibers/epoxy interfacial adhesion, Appl. Surf. Sci. 257 (2011) 6980–6985. https://doi.org/10.1016/j.apsusc.2011.03.047.
[41] S.R. Taylor, Coatings for Corrosion Protection: Inorganic, in: Encyclopedia of Materials: Science and Technology, Elsevier, 2001: pp. 1263–1269. https://doi.org/10.1016/B0-08-043152-6/00238-2.

[42] H. Touhara, F. Okino, Property control of carbon materials by fluorination, Carbon. 38 (2000) 241–267. https://doi.org/10.1016/S0008-6223(99)00140-2.
[43] L. Fischer, U. Siemann, W. Ruland, Structure and properties of fluorinated carbon fibers, Colloid Polym. Sci. 261 (1983) 744–749. https://doi.org/10.1007/BF01410948.
[44] S. Cholake, M. Mada, R. Raman, Y. Bai, X. Zhao, S. Rizkalla, S. Bandyopadhyay, Quantitative Analysis of Curing Mechanisms of Epoxy Resin by Mid- and Near- Fourier Transform Infra Red Spectroscopy, Def Sci J. 64 (2014) 314–321. https://doi.org/10.14429/dsj.64.7326.
[45] S. Jiang, P. Huang, J. Lu, Z. Liu, Fluorination of Carbon Molecular Sieve as Cathode Material for Lithium Primary Batteries and its Characteristics, E3S Web Conf. 245 (2021) 01009. https://doi.org/10.1051/e3sconf/202124501009.
[46] S. Jiang, P. Huang, J. Lu, Z. Liu, Fluorinated Ketjen-black as Cathode Material for Lithium Primary Batteries, E3S Web Conf. 218 (2020) 02021. https://doi.org/10.1051/e3sconf/202021802021.
[47] Y. Kita, N. Watanabe, Y. Fujii, Chemical composition and crystal structure of graphite fluoride, J. Am. Chem. Soc. 101 (1979) 3832–3841. https://doi.org/10.1021/ja00508a020.
[48] M. Dubois, J. Giraudet, K. Guérin, A. Hamwi, Z. Fawal, P. Pirotte, F. Masin, EPR and Solid-State NMR Studies of Poly(dicarbon monofluoride) $(C_2F)_n$, J. Phys. Chem. B. 110 (2006) 11800–11808. https://doi.org/10.1021/jp061291m.
[49] Z.Q. Li, C.J. Lu, Z.P. Xia, Y. Zhou, Z. Luo, X-ray diffraction patterns of graphite and turbostratic carbon, Carbon. 45 (2007) 1686–1695. https://doi.org/10.1016/j.carbon.2007.03.038.
[50] J.I. Langford, A.J.C. Wilson, Scherrer after Sixty Years: A Survey and Some New Results in the Determination of Crystallite Size, J. Appl. Cryst. (1978) 102–113. https://doi.org/10.1107/S0021889878012844.
[51] Y. Sato, K. Itoh, R. Hagiwara, T. Fukunaga, Y. Ito, Short-range structures of poly(dicarbon monofluoride) (C2F)n and poly(carbon monofluoride) (CF)n, Carbon. 42 (2004) 2897–2903. https://doi.org/10.1016/j.carbon.2004.06.042.
[52] A. Merlen, J. Buijnsters, C. Pardanaud, A Guide to and Review of the Use of Multiwavelength Raman Spectroscopy for Characterizing Defective Aromatic Carbon Solids: from Graphene to Amorphous Carbons, Coatings. 7 (2017) 153. https://doi.org/10.3390/coatings7100153.
[53] A.C. Ferrari, J. Robertson, Interpretation of Raman spectra of disordered and amorphous carbon, Phys. Rev. B. 61 (2000) 14095–14107. https://doi.org/10.1103/PhysRevB.61.14095.
[54] C. Pardanaud, C. Martin, P. Roubin, Multiwavelength Raman spectroscopy analysis of a large sampling of disordered carbons extracted from the Tore Supra tokamak, Vib. Spectrosc. 70 (2014) 187–192. https://doi.org/10.1016/j.vibspec.2013.12.004.
[55] C. Sisu, R. Iordanescu, V. Stanciu, I. Stefanescu, A.M. Vlaicu, V.V. Grecu, Raman Spectroscopy Studies of some Carbon Molecular Sieves, Dig. J. Nanomater. Biostructures. 11 (2016) 435–442.
[56] I.P. Asanov, L.G. Bulusheva, M. Dubois, N.F. Yudanov, A.V. Alexeev, T.L. Makarova, A.V. Okotrub, Graphene nanochains and nanoislands in the layers of room-temperature fluorinated graphite, Carbon. 59 (2013) 518–529. https://doi.org/10.1016/j.carbon.2013.03.048.
[57] J.T. Robinson, J.S. Burgess, C.E. Junkermeier, S.C. Badescu, T.L. Reinecke, F.K. Perkins, M.K. Zalalutdniov, J.W. Baldwin, J.C. Culbertson, P.E. Sheehan, E.S. Snow, Properties of Fluorinated Graphene Films, Nano Lett. 10 (2010) 3001–3005. https://doi.org/10.1021/nl101437p.

[58] C. Matei Ghimbeu, K. Guerin, M. Dubois, S. Hajjar-Garreau, C. Vix-Guterl, Insights on the reactivity of ordered porous carbons exposed to different fluorinating agents and conditions, Carbon. 84 (2015) 567–583. https://doi.org/10.1016/j.carbon.2014.12.034.
[59] F. Chamssedine, M. Dubois, K. Guérin, J. Giraudet, F. Masin, D.A. Ivanov, L. Vidal, R. Yazami, A. Hamwi, Reactivity of Carbon Nanofibers with Fluorine Gas, Chem. Mater. 19 (2007) 161–172. https://doi.org/10.1021/cm061731m.
[60] M. Panich, A.I. Shames, T. Nakajima, On paramagnetism in fluorinated graphite: EPR and solid state NMR study, J. Phys. Chem. Solids. 62 (2001) 959–964. https://doi.org/10.1016/S0022-3697(00)00264-X.
[61] W. Zhang, K. Guérin, M. Dubois, Z.E. Fawal, D.A. Ivanov, L. Vidal, A. Hamwi, Carbon nanofibres fluorinated using TbF4 as fluorinating agent. Part I: Structural properties, Carbon. 46 (2008) 1010–1016. https://doi.org/10.1016/j.carbon.2008.02.029.
[62] A. Tressaud, E. Durand, C. Labrugère, A.P. Kharitonov, L.N. Kharitonova, Modification of surface properties of carbon-based and polymeric materials through fluorination routes: From fundamental research to industrial applications, J. Fluorine Chem. 128 (2007) 378–391. https://doi.org/10.1016/j.jfluchem.2006.12.015.
[63] A. Hamwi, R. Yazami, Fluorination of Multi-Layered Carbon Nanomaterials, US 7,794,880 B2, 2010.
[64] N.S. Broyles, R. Chan, R.M. Davis, J.J. Lesko, J.S. Riffle, Sizing of carbon fibres with aqueous solutions of poly(vinyl pyrollidone), Polymer. 39 (1998) 2607–2613. https://doi.org/10.1016/S0032-3861(97)00562-4.
[65] M. Dubois, K. Guérin, Y. Ahmad, N. Batisse, M. Mar, L. Frezet, W. Hourani, J.-L. Bubendorff, J. Parmentier, S. Hajjar-Garreau, L. Simon, Thermal exfoliation of fluorinated graphite, Carbon. 77 (2014) 688–704. https://doi.org/10.1016/j.carbon.2014.05.074.
[66] M. Herraiz, M. Dubois, N. Batisse, S. Hajjar-Garreau, L. Simon, Large-scale synthesis of fluorinated graphene by rapid thermal exfoliation of highly fluorinated graphite, Dalton Trans. 47 (2018) 4596–4606. https://doi.org/10.1039/C7DT04565D.
[67] A. Tressaud, T. Shirasaki, G. Nansé, E. Papirer, Fluorinated carbon blacks: influence of the morphology of the starting material on the fluorination mechanism, Carbon. 40 (2002) 217–220. https://doi.org/10.1016/S0008-6223(01)00177-4.
[68] A.P. Kharitonov, Direct fluorination of polymers - From fundamental research to industrial applications, Prog. Org. Coat. 61 (2008) 192–204. https://doi.org/10.1016/j.porgcoat.2007.09.027.
[69] A.P. Kharitonov, R. Taege, G. Ferrier, N.P. Piven, The kinetics and mechanism of the direct fluorination of polyethylenes, Surf. Coat. Int. B: Coat. Trans. 88 (2005) 201–212. https://doi.org/10.1007/BF02699574.
[70] D.K. Owens, R.C. Wendt, Estimation of the surface free energy of polymers, J. Appl. Polym. Sci. 13 (1969) 1741–1747. https://doi.org/10.1002/app.1969.070130815.
[71] K. Song, J. Lee, S.-O. Choi, J. Kim, Interaction of Surface Energy Components between Solid and Liquid on Wettability, and Its Application to Textile Anti-Wetting Finish, Polymers. 11 (2019) 498. https://doi.org/10.3390/polym11030498.
[72] M.F. Pucci, P.-J. Liotier, D. Seveno, C. Fuentes, A. Van Vuure, S. Drapier, Wetting and swelling property modifications of elementary flax fibres and their effects on the Liquid Composite Molding process, Compos. Part A Appl. Sci. Manuf. 97 (2017) 31–40. https://doi.org/10.1016/j.compositesa.2017.02.028.
[73] M. Dubois, N. Batisse, K. Guérin, P. Thomas, Fluorine: Characteristics, Chemistry and Applications Controlled fluorination using atomic fluorine, in: A. Huff (Ed.), Chemical Elements (Fluorine, Rhodium and Rubidium): Properties, Synthesis and Applications, Nova Science Publishers, 2018.

[74] R.B. Mathur, V. Gupta, O.P. Bahl, A. Tressaud, S. Flandrois, Improvement in the mechanical properties of polyacrylonitrile (PAN)- based carbon fibers after fluorination, Synth. Met. 114 (2000) 197–200. https://doi.org/10.1016/S0379-6779(00)00251-4.
[75] L.C. Pardini, L.G.B. Manhani, Influence of the Testing Gage Length on the Strength, Young's Modulus and Weibull Modulus of Carbon Fibres and Glass Fibres, Mat. Res. 5 (2002) 411–420. https://doi.org/10.1590/S1516-14392002000400004.
[76] K. Naito, J.-M. Yang, Y. Inoue, H. Fukuda, The effect of surface modification with carbon nanotubes upon the tensile strength and Weibull modulus of carbon fibers, J Mater Sci. 47 (2012) 8044–8051. https://doi.org/10.1007/s10853-012-6694-6.
[77] N. Tudorachi, F. Mustata, Curing and thermal degradation of diglycidyl ether of bisphenol A epoxy resin crosslinked with natural hydroxy acids as environmentally friendly hardeners, Arab. J. Chem. 13 (2020) 671–682. https://doi.org/10.1016/j.arabjc.2017.07.008.
[78] A.K. Kuriakose, J.L. Margrave, Mass Spectrometric Studies of the Thermal Decomposition of Poly(carbon monofluoride), Inorg. Chem. 4 (1965) 1639–1641. https://doi.org/10.1021/ic50033a023.

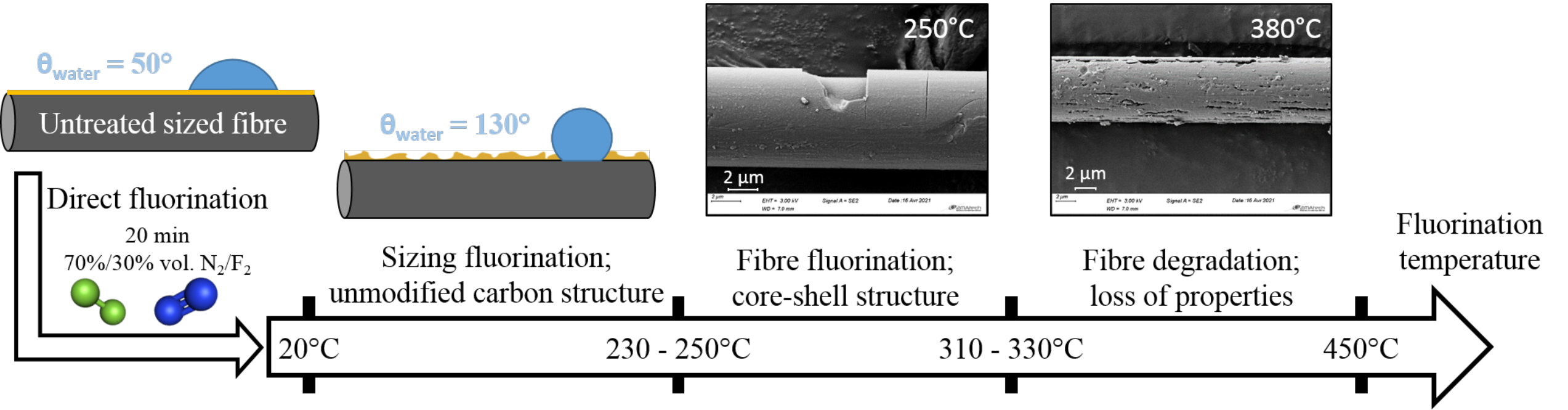
θwater = 50°
Untreated sized fibre
Direct fluorination
20 min
70%/30% vol. N2/F2
θwater = 130°
250°C
2 µm
380°C
2 µm
Sizing fluorination;
unmodified carbon structure
Fibre fluorination;
core-shell structure
Fibre degradation;
loss of properties
Fluorination
temperature
20°C
230 - 250°C
310 - 330°C
450°C